

Unique selectivity reversal in actinide – lanthanide extraction in a tripodal TREN-based diglycolamide in ionic liquid: Extraction, luminescence, complexation and structural studies

Andrea Leoncini,^a Prasanta K. Mohapatra,^{b,*} Arunasis Bhattacharyya,^b Dhaval R. Raut,^b Arijit Sengupta,^b Parveen K. Verma,^b Nidhi Tiwari,^c Dibyendu Bhattacharyya,^c Sambhunath Jha,^c Anna M. Wouda,^a Jurriaan Huskens^a and Willem Verboom^{a,*}

^aLaboratory of Molecular Nanofabrication, MESA+ Institute for Nanotechnology, University of Twente, P.O. Box 217, 7500 AE Enschede, The Netherlands

^bRadiochemistry Division, Bhabha Atomic Research Centre, Trombay, Mumbai-400085, India

^cAtomic & Molecular Physics Division, Bhabha Atomic Research Centre, Trombay, Mumbai-400085, India

Electronic Supplementary Information

Contents

Spectra of DGA-TREN	3
Solvent extraction studies	5
Stripping data	6
IR and ¹H-NMR spectra of LaTf₃ complexes of DGA-TREN in toluene-<i>d</i>₈	7
Luminescence studies	9
EXAFS studies	14
References	18

Spectra of DGA-TREN

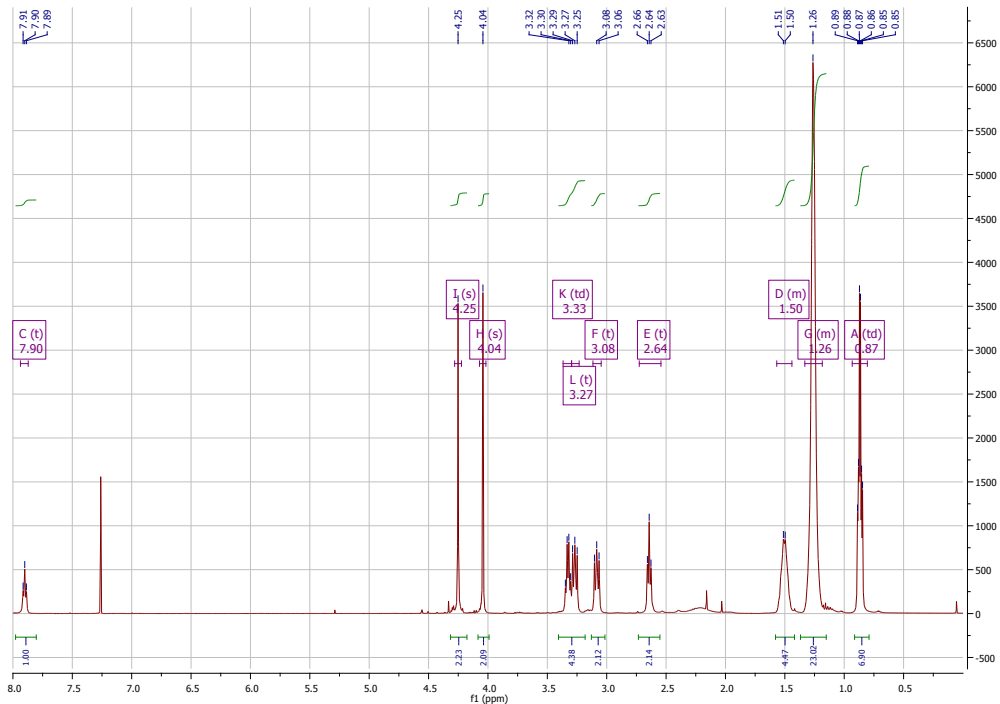


Fig. S1 ^1H -NMR spectrum of DGA-TREN in CDCl_3

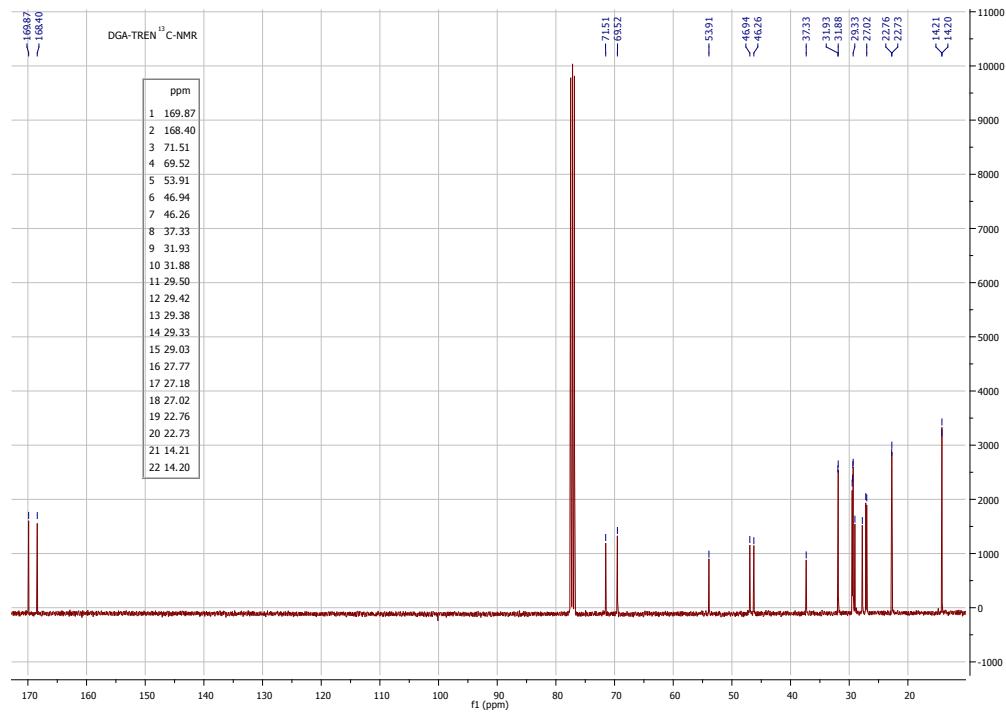


Fig. S2 ^{13}C -NMR spectrum of DGA-TREN in CDCl_3

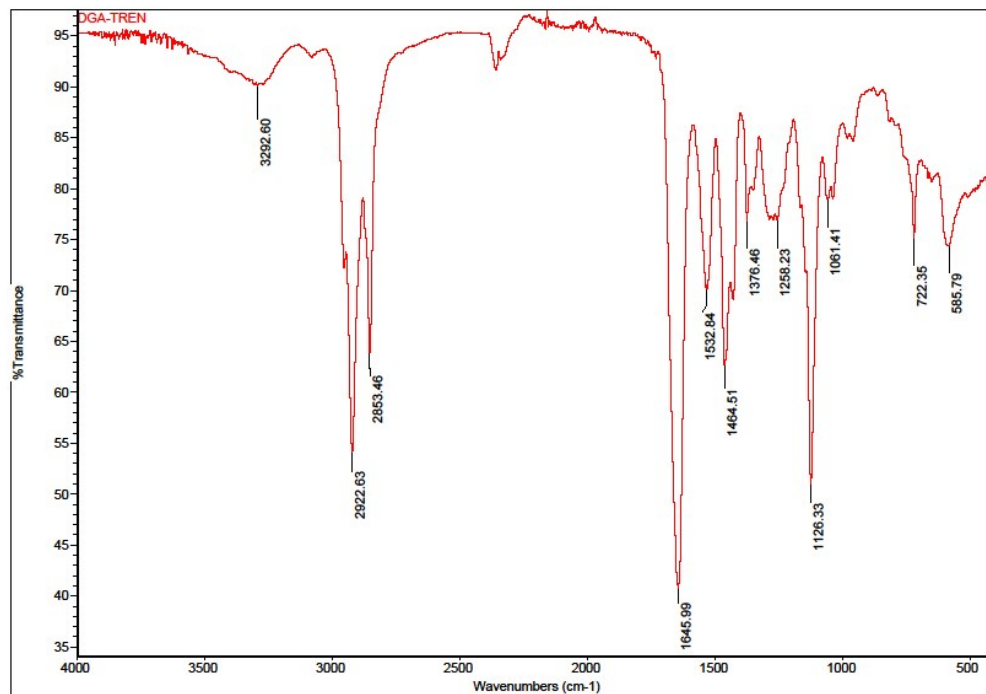


Fig. S3 FT-IR spectrum of DGA-TREN (pure)

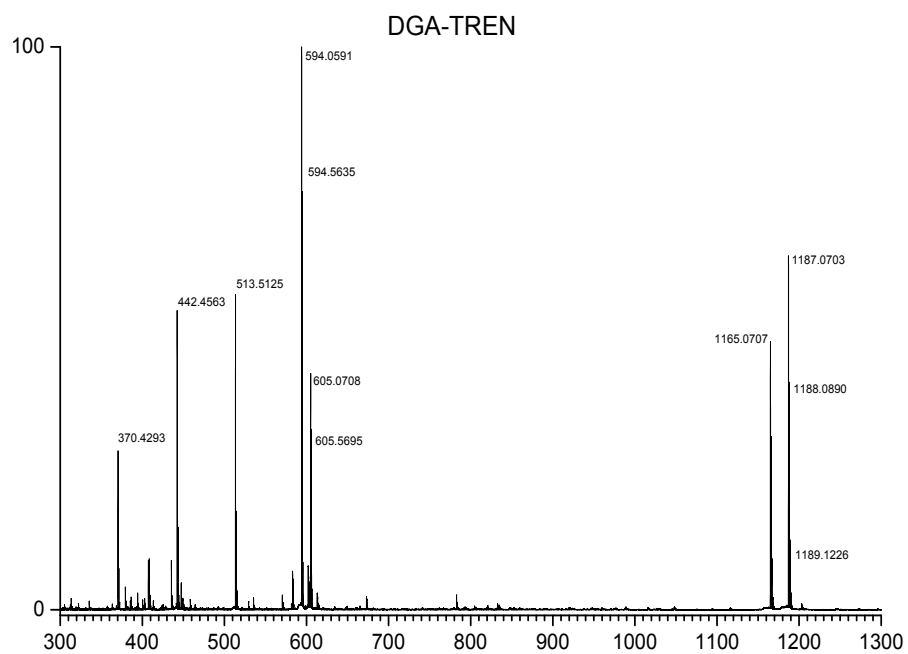


Fig. S4 ESI-MS spectrum of DGA-TREN

Solvent extraction studies

Equilibration time

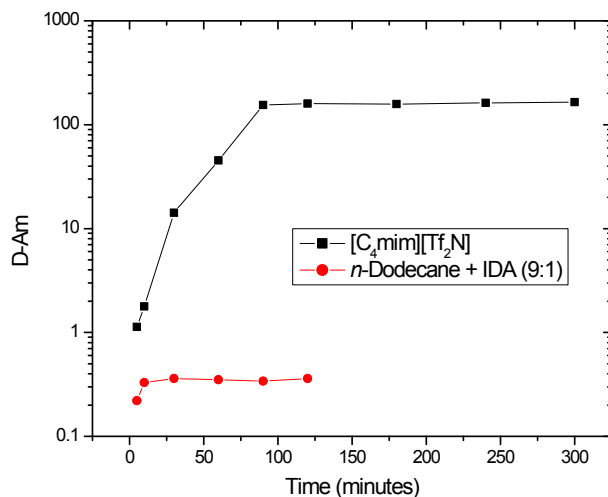


Fig. S5 Equilibration time optimization study for the extraction of Am(III) using DGA-TREN (1.0×10^{-3} M) in molecular diluents (circle) and ionic liquid (square). Aqueous phase: 3 M HNO₃

Slope analysis to determine the nature of extracted species

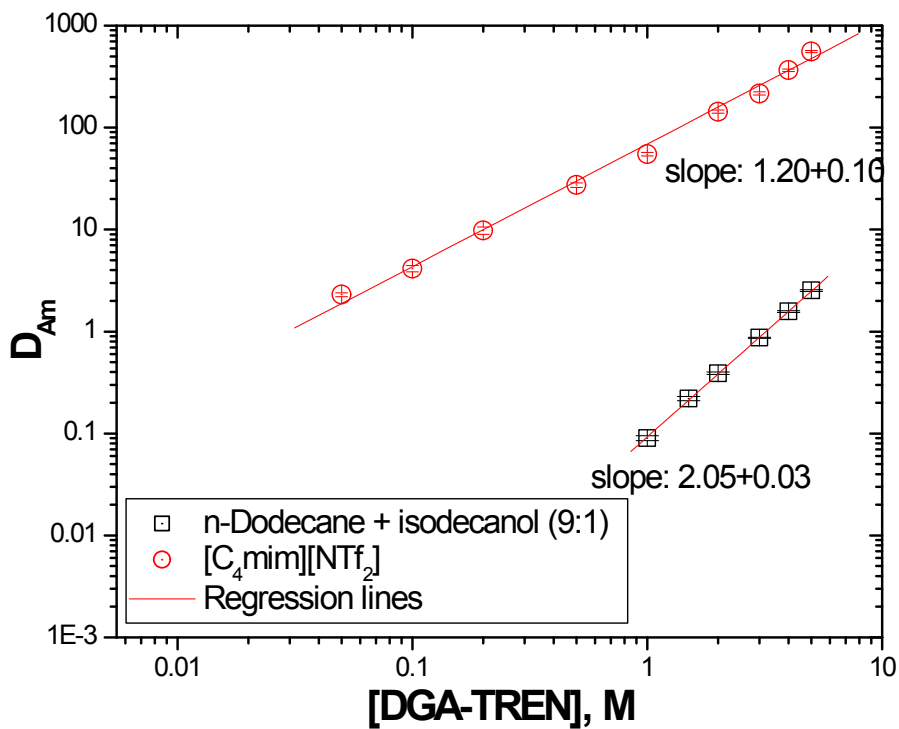


Fig. S6 Plots of log D vs log [DGA-TREN] at 3 M HNO₃

Stripping studies

Table S1 Conditions for quantitative stripping of Am(III) from the loaded organic phase containing 1 mM DGA-TREN

Strippant	Diluent	No. of stages required for >99.9% stripping
Buffer mixture	Mol. diluent mixture	2
pH 2	Mol. diluent mixture	2
Buffer mixture	[C ₄ mim][NTf ₂]	4
0.05 M EDTA + 1 M guanidine carbonate	[C ₄ mim][NTf ₂]	2

IR and $^1\text{H-NMR}$ spectra of LaTf_3 complexes of DGA-TREN in toluene- d_8

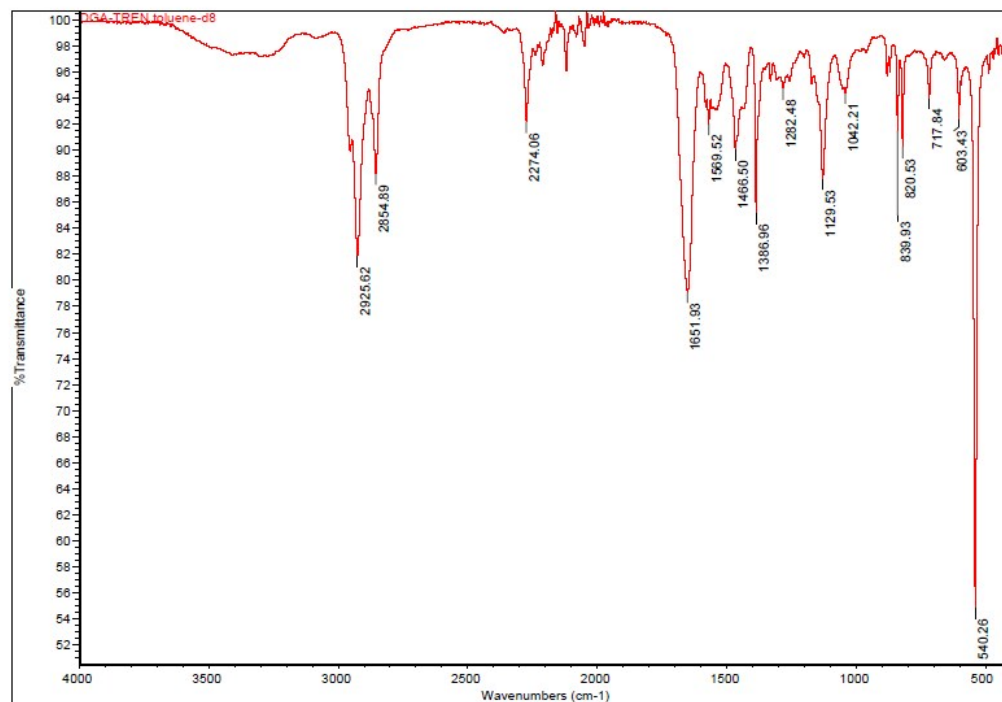


Fig. S7 FT-IR spectrum of free DGA-TREN in toluene- d_8

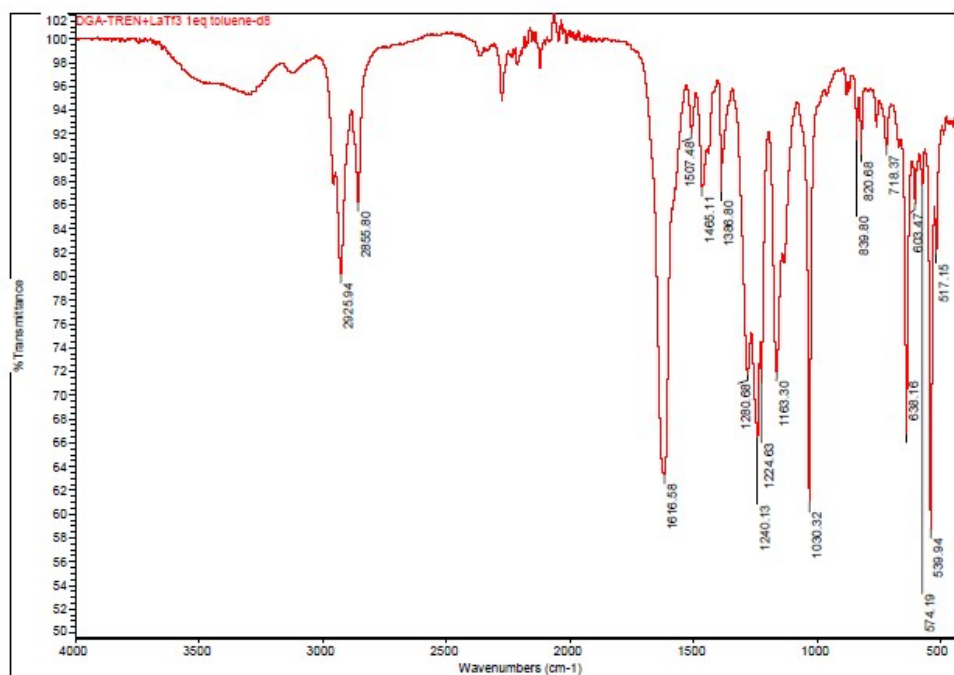


Fig. S8 FT-IR spectrum of the 1:1 lanthanum triflate complex of DGA-TREN in toluene- d_8

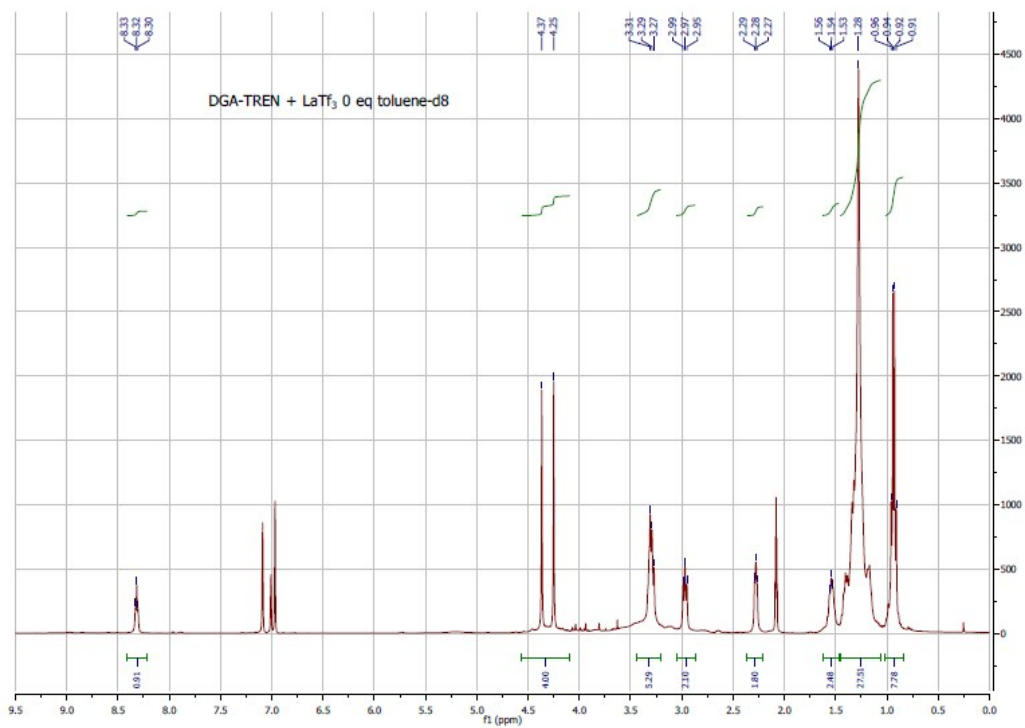


Fig. S9 ¹H-NMR spectrum of free DGA-TREN in toluene-*d*₈

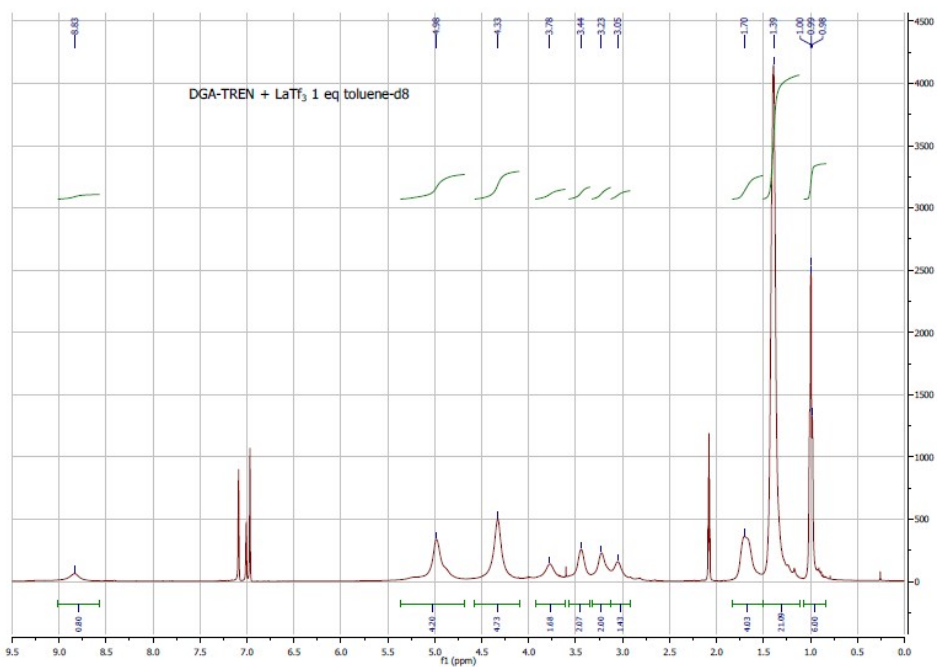


Fig. S10 ¹H-NMR spectrum of the lanthanum triflate complex of DGA-TREN in toluene-*d*₈ with a metal to ligand ratio of 1:1

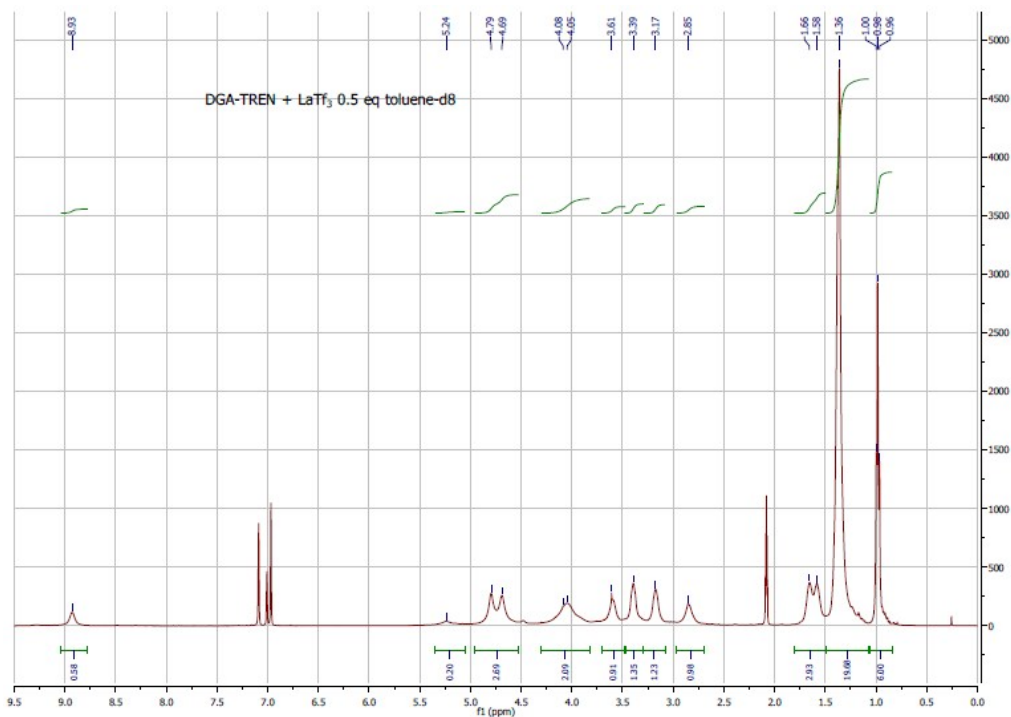


Fig. S11 ^1H -NMR spectrum of the lanthanum triflate complex of DGA-TREN in toluene- d_8 with a metal to ligand ratio of 1:2

Luminescence studies

Results

A luminescence spectroscopic investigation was carried out to understand the nature of the complex of Eu^{3+} with DGA-TREN both in the molecular diluent and in the ionic liquid $[\text{C}_4\text{mim}][\text{Tf}_2\text{N}]$. In the luminescence profiles of the Eu complexes (Fig. 3 in the main text), five sets of emission lines were assigned to the particular transition (1st set at ~ 580 nm - $^5\text{D}_0$ - $^7\text{F}_0$ transition, 2nd set at ~ 593 nm - $^5\text{D}_0$ - $^7\text{F}_1$ transition, 3rd set at ~ 613 nm - $^5\text{D}_0$ - $^7\text{F}_2$ transition, 4th set at ~ 650 nm - $^5\text{D}_0$ - $^7\text{F}_3$ transition, and 5th set at ~ 700 nm - $^5\text{D}_0$ - $^7\text{F}_4$ transition).¹ The $^5\text{D}_0$ - $^7\text{F}_2$ transition, being an electric dipole transition is hypersensitive with the ligand field, while the

5D_0 - 7F_1 transition, being a magnetic dipole transition is insensitive, reflected in the transition probabilities summarized in Table S2.

Table S2 Photophysical properties of the Eu^{3+} - DGA-TREN complex in $[\text{C}_4\text{mim}][\text{Tf}_2\text{N}]$ and molecular diluent

System	$[\text{C}_4\text{mim}][\text{Tf}_2\text{N}]$	Molecular diluent
\dot{U}_2	4.79E-20	4.43E-20
\dot{U}_4	3.57E-20	5.77E-20
$\hat{\sigma}_R$ (sec)	4.38E-3	4.67E-3
$\hat{\sigma}_{NR}$ (sec)	2.46E-3	2.46E-3
ζ	3.59E-1	2.22E-1
A	2.91	2.70
Lifetime (ms)	1.575	1.037
$N_{\text{H}_2\text{O}}$	0	0
N_{ligand}	1	2
\hat{a}_1	1.87E-1	1.64E-1
\hat{a}_2	5.45E-1	4.44E-1
\hat{a}_4	2.04E-1	2.93E-1
A_{md}	4.26E+1	4.11E+1
$A_{2\text{ed}}$	1.24E+2	0.95E+2
$A_{4\text{ed}}$	4.67E+1	6.27E+1

The **excitation** profiles of the Eu^{3+} -DGA-TREN complex in both the molecular diluent and in the ionic liquid $[\text{C}_4\text{mim}][\text{Tf}_2\text{N}]$ are given in Fig. S12. Absorption bands resolved in the UV–vis range correspond to the 7F_0 - 5D_2 , $^5G_{2,3,4}$, 5L_6 and 7F_1 - 5D_2 transitions. All assignments of transitions are based on assignments of lanthanide spectra from literature.² The close proximity of the $^7F_{1,2}$ states of Eu^{3+} to its ground state 7F_0 , their separation being ~ 250 and ~ 1000 cm^{-1} , respectively, from the ground state, makes these states adequately populated even at room temperature. This enables **excitation** from $^7F_{0,1,2}$ states of Eu^{3+} to excited states. Although forbidden by the ΔS and ΔL selection rule, the transition (7F_0 - 5L_6) is allowed by the ΔJ rule.

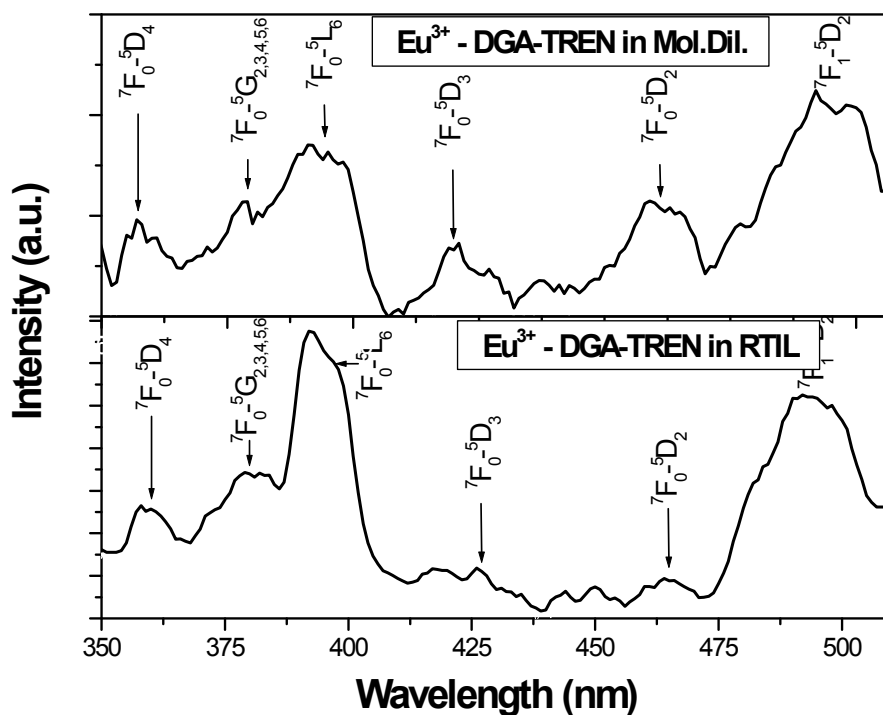


Fig. S12 Excitation spectra of Eu^{3+} - DGA-TREN

Titration studies to calculate complexation constants

To understand the complexation, titration of Eu^{3+} with DGA-TREN was carried out in [methanol – water mixture](#) using luminescence as a tool (Fig. S13). Fig. S14 represents the Job's plot indicating the enhancement of the luminescence intensity upon complexation. It also shows that the species of $L:M = 2$ differ from that of $L:M = 1:1$. In the same phase complexation, upon increase of the relative mole fraction of the ligand, the intensity of the hypersensitive ${}^5\text{D}_0$ - ${}^7\text{F}_2$ transition initially increases, followed by an inflection point. The inflection point indicates the nature of the complex to be $L:M = 2:1$ (formation constant, $\log \beta = 9.6 \pm 0.5$) (Fig. S13). The asymmetry factor also increased upon addition of DGA-TREN, suggesting a change of the nature of the complex to $L:M = 2:1$. Beyond that, it remained almost unchanged suggesting the formation of single species with $L:M = 2:1$.

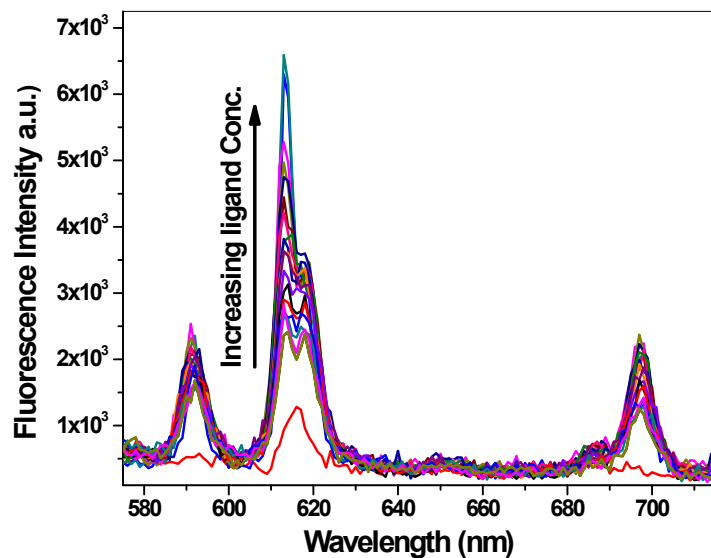


Fig. S13 Change in fluorescence spectra of Eu³⁺ with increasing complexation with DGA-TREN

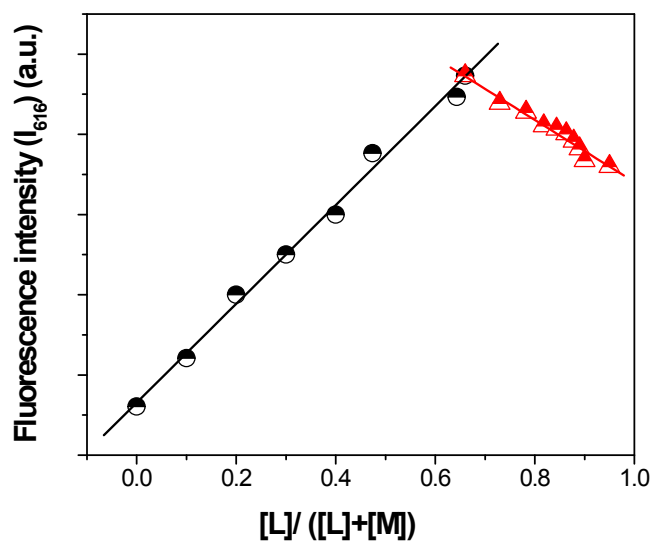
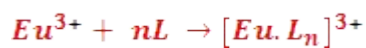


Fig. S14 Job's plot of DGA-TREN and Eu³⁺ in CH₃OH-H₂O mixture. The emission intensity at 616 nm is plotted against the molar fraction of [DGA-TREN] to ([DGA-TREN] + [Eu³⁺]) ($\lambda_{\text{ex}} = 394$ nm). $[L]/([L]+[M]) = 0.65$ implying L:M = 2:1. $\text{Log } \beta = 9.6 \pm 0.5$



$$\beta = \frac{[Eu \cdot L_n]^{3+}}{[Eu]_{free}^{3+} \cdot [L]^n}$$

$$\log \left[\frac{[Eu]_{complex}}{[Eu]_{free}} \right] = \log \beta + n \log [L]$$

where, $[Eu]_{complex}$ is the europium ion complexed with N-TDGA, $[Eu]_{free}$ is the free europium ion concentration, n is metal ligand stoichiometry and β is the conditional stability constant. When M:L is < 2, then the overall luminescence intensity is due to the complexed Eu^{3+} ion while when the relative ratio of M:L > 2, then the overall luminescence intensity is a combination of complexed Eu^{3+} and uncomplexed Eu^{3+} .

EXAFS studies

The experimental EXAFS ($\mu(E)$ versus E) spectrum of the complex, which is a merged spectrum of several scans, is shown in Fig. S15. The energy dependent absorption coefficient $\mu(E)$ was converted into the absorption function $\chi(E)$, defined as expressed in equation (1),³ to take care of the oscillations in the absorption spectra:

$$\chi(E) = \frac{\mu(E) - \mu_0(E)}{\Delta\mu_0(E_0)} \quad (1)$$

where E_0 is the energy at the absorption edge, $\mu_0(E_0)$ represents the bare atom background and $\Delta\mu_0(E_0)$ is the step in the $\mu(E)$ value at the Eu(III) absorption edge. The energy scale was converted into the photoelectron wavenumber scale (k) by using equation (2):

$$k = \sqrt{\frac{2m(E - E_0)}{h^2}} \quad (2)$$

The goodness of the data fit with experimental spectra was determined by the value of the R_{factor} defined by equation (3):

$$R_{factor} = \sum \frac{[\text{Im}(\chi_{dat}(r_i) - \chi_{th}(r_i))]^2 + [\text{Re}(\chi_{dat}(r_i) - \chi_{th}(r_i))]^2}{[\text{Im}(\chi_{dat}(r_i))]^2 + [\text{Re}(\chi_{dat}(r_i))]^2} \quad (3)$$

where χ_{dat} and χ_{th} refer to the experimental and theoretical $\chi(r)$ values, respectively, and Re and Im refer to the real and imaginary parts of the respective quantities.

The energy dependent absorption function $\chi(E)$ was converted into the wavenumber dependent absorption function $\chi(k)$, where m is the mass of an electron. Finally, $\chi(k)$ is weighted by k^2 to amplify the oscillation at higher k and the $k^2 \chi(k)$ functions are Fourier transformed in real or R space to generate the $\chi(R)$ versus R plots (or FT-EXAFS spectra) in terms of the actual distances from the center of the absorbing atom. A set of EXAFS data analysis programs, available within the IFEFFIT software package, were used for background correction, normalization and fitting of the experimental EXAFS data.⁴ The ATHENA software was used for data reduction and Fourier transform to derive the $\chi(R)$ versus R spectra from the absorption spectra. The ARTEMIS software was used for generation of the theoretical EXAFS spectra starting from an assumed crystallographic structure and final fitting of the experimental

data with the theoretical spectra using the FEFF 6.0 code. For the present sample the k range used for Fourier transform is 2-11 \AA^{-1} .

In the manuscript, Fig. 7 represents $k^2\chi(k)$ vs. k (bottom) and $\chi(R)$ versus R plots (top) of the Eu-DGA-TREN complex at the EuL_3 edge along with the best fit theoretical plots generated by taking two possible structures. It should be noted here that in Fig. 7 the R scale does not represent the actual distance from the absorbing atom because of the presence of an EXAFS phase shift. In both the guess structures, 1:2 metal to ligand stoichiometry with three nitrates ($\text{EuC}_{48}\text{N}_{17}\text{H}_{90}\text{O}_{27}$) was assumed with a difference in the mode of nitrate binding to Eu(III) , viz., Structure-1: all nitrates are monodentate, whereas in the second structure, Structure-2: two nitrates are bidentate and one is monodentate. In both cases the data were fitted up to 3.5 \AA in R space and it was assumed that the first major peak in the radial distribution function corresponds to the two oxygen shells ($\text{O}_{\text{Nitrate}}$, $\text{O}_{\text{Carbonyl}}$), the second peak to one $\text{O}_{\text{Etherial}}$ shell, while the third peak corresponds to the combined contributions of the nitrogen and carbon shells.

(i) Results of fitting using Structure-1. In this formalism, based on the inputs from theoretical calculations, the theoretical EXAFS spectra were generated by assuming the first oxygen shell $\text{O}_{\text{Nitrate}}$ at 2.39 \AA with a CN of 3 from the nitrate groups, the second oxygen shell $\text{O}_{\text{carbonyl}}$ at 2.44 \AA with a CN of 4 from the carbonyl groups, the third oxygen shell at 2.82 \AA having a CN of 2 from the etherial groups, the fourth nitrogen shell at 3.42 \AA with a CN of 3 from the nitrate groups and the fifth carbon shell at 3.69 \AA with a CN of 8 from the combined carbonyl groups and the etherial carbons. From Table S3 it is clear that in this case, the oxygen coordinations of the first and third oxygen shells are higher than their theoretical values, while the carbon coordination is similar to its theoretical values.

(ii) Results of fitting using Structure-2: From the inputs obtained from theoretical calculations, the theoretical EXAFS spectra were generated by assuming the $\text{O}_{\text{Nitrate}}$ oxygen shell at 2.56 \AA with a CN of 5, the $\text{O}_{\text{Carbonyl}}$ oxygen shell at 2.52 \AA with a CN of 4 from the carbonyl groups, the third oxygen shell at 2.65 \AA having a CN of 1 from the ether groups as the second etherial oxygen was very far away (3.88 \AA) for bonibing interactions, a nitrogen shell at 2.90 \AA with a CN of 2 from the two nitrate groups and a carbon (from carbonyl and etherial carbons) and nitrogen shell (from nitrate) at 3.45 \AA with a CN of 9 (8 carbon + 1 nitrogen). Since oxygen

coordinations of the first shell obtained from the fitting carried out by both the above structures are found to be significantly higher, fitting was carried out using another formalism, where the values of the Debye-Waller Factors (σ^2) of this shell is kept intentionally low, which results in lower values of the coordination numbers. The fitting result shows a poor fitting (large R -factor) of experimental data for structure-2 with an unrealistic coordination number for both nitrogen and carbon, as compared to structure-1. The bond length, derived from theoretical and EXAFS studies, matches well with structure-1 and less with structure-2. However, the overall fitting results of Fig. 5 do not show a very poor fit of the data along with high values of the R -factor.

Table S3 EXAFS fitted - structural parameters for the Eu³⁺-DGA-TREN complex with the two possible structures discussed in the text

	PKV:3 Eu Structure 1 (EuC ₄₈ N ₁₇ H ₉₀ O ₂₇)			PKV:3 Eu Structure 2 (EuC ₄₈ N ₁₆ H ₉₀ O ₂₄)
Eu-O1	CN(4)	6.6 ± 0.96	CN(9)	7.29 ± 0.65
	R	2.32 ± 0.008	R	2.35 ± 0.008
	σ ²	0.001 ± 0.0008	σ ²	0.005 ± 0.003
	S ₀ ²	0.81	S ₀ ²	0.81
	ΔE ₀	1.96	ΔE ₀	1.96
Eu-O2	CN(4)	2.76 ± 0.52	CN(2)	1.44 ± 0.62
	R	2.45 ± 0.02	R	2.41 ± 0.03
	σ ²	0.002 ± 0.002	σ ²	0.003
	S ₀ ²	0.72	S ₀ ²	0.72
	ΔE ₀	1.96	ΔE ₀	1.96
Eu-O3	CN(2)	2.92 ± 0.44	--	--
	R	2.99 ± 0.007	--	--
	σ ²	0.002 ± 0.001	--	--
	S ₀ ²	1.46	--	--
	ΔE ₀	1.96	--	--
Eu-N	CN(3)	3	CN(3)	6.9 ± 1.4
	R	3.55 ± 0.07	R	2.8 ± 0.05
	σ ²	0.005 ± 0.0007	σ ²	0.004 ± 0.003
	S ₀ ²	1	S ₀ ²	1
	ΔE ₀	1.96	ΔE ₀	1.96
Eu-C	CN(8)	7.68 ± 0.79	CN(8)	14.4 ± 1.52
	R	3.8 ± 0.01	R	3.48 ± 0.014
	σ ²	0.006 ± 0.0009	σ ²	0.002 ± 0.001
	S ₀ ²	1	S ₀ ²	1
	ΔE ₀	1.96	ΔE ₀	1.96
R-Factor		0.002		0.001

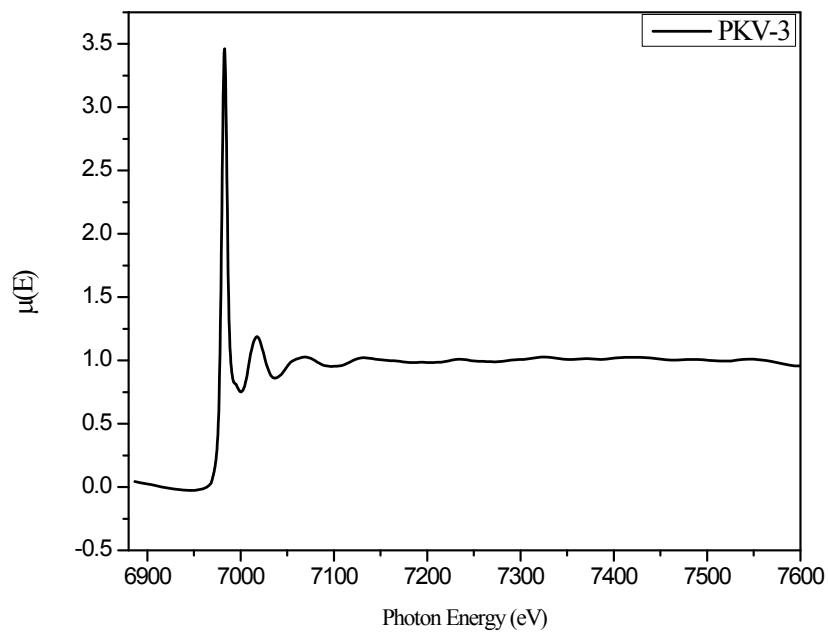


Fig. S15 Normalized experimental EuL₃-edge EXAFS ($\mu(E)$ versus E) spectrum of the Eu-DGA-TREN complex at 298 K

References

1. B. Boulon, M. Bourderbala and J. Seriot, *J. Less-Common. Mat.*, **1985**, *112*, 41-66.
2. (a) G. H. Dieke, *Spectroscopy & Energy Levels of Rare Earth Compounds*, Inter Science, New York, 1968; (b) W. T. Carnall, P. R. Fields and K. Rajnak, *J. Chem. Phys.*, **1968**, *49*, 4412-4428.
3. *X-Ray Absorption: Principles, Applications, Techniques of EXAFS, SEXAFS and XANES*, edited by D. C. Konigsberger and R. Prince (Wiley, New York, 1988).
4. M. Newville, B. Ravel, D. Haskel, J. J. Rehr, E. A. Stern and Y. Yacoby, *Physica B*, **1995**, *208-209*, 154-156.